Microhardness-fracture studies: high alumina cement systems
Beaudoin, J. J.

National Research Council Canada   Conseil national de recherches Canada

Canada

10467

National Research Conseil national
Council Canada de recherches Canada

MICROHARDNESS-FRACTURE STUDIES:

HIGH ALUMINA CEMENT SYSTEMS

by J. J. Beaudoin

ANALYZED

11584

Price $1.25 OTTAWA NRCC 20377

Canada

MICROHARDNESS-FRACTURE STUDIES: HIGH ALUMINA CEMENT SYSTEMS
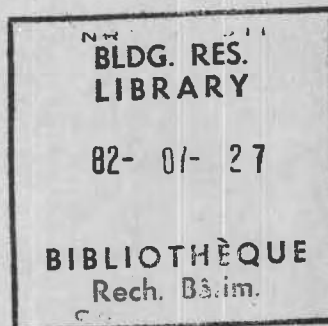
J.J. Beaudoin
Division of Building Research, National Research Council of Canada, Ottawa
Canada K1A OR6

Microhardness and fracture parameters of several high alumina cement
paste systems containing varying proportions of hexagonal and cubic
phases have been determined using single edge-notched flexural
specimens from each system. Specimens were conditioned and tested at
11% RH in a specially constructed environmental chamber. Data
demonstrated dependence of the fracture parameters on microhardness.
Effect of morphology and other microstructural features on fracture in
HAC paste is also discussed. Some evidence supporting argument for
the validity of applying linear-elastic fracture mechanics in studying
fracture in brittle cementitious systems is presented.

RESUME

À partir d'éprouvettes à encoche périphérique simple pour essais de
flexion, on a déterminé les paramètres de microdureté et de rupture de
plusieurs systèmes de pâte de ciment alumineux contenant différentes
proportions de phases hexagonales et cubiques. Les éprouvettes ont
été conditionnées et mises à l'essai à 11% d'humidité relative dans un
contenant spécialement construit à cet effet. Les données ont montré
que les paramètres de rupture étaient fonction de la microdureté. On
examine aussi l'effet de la morphologie et autres caractéristiques de
la microstructure sur la rupture dans la pâte de ciment alumineux. On
présente des faits venant corroborer l'argument selon lequel il est
valable d'employer la mécanique de rupture linéaire-élastique pour
étudier la rupture dans les systèmes de liants fragiles.

Introduction

High alumina cement (HAC) consists of approximately equal parts of alumina
and lime, about 40% each, with ferrous and ferric oxides and up to 5% silica.
It comprises several phases, viz., CA, CA_2, $C_{12}A_7$, C_2AS, C_2S, C_2F and C_4AF,
but the main cementitious compounds are CA and $C_{12}A_7$.* The hydration

---

*In cement chemistry nomenclature: $C = CaO$, $A = Al_2O_3$, $S = SiO_2$, $F = Fe_2O_3$,
$H = H_2O$.

J.J. Beaudoin

products of CA consist of CAH_{10}, C_2AH_8, C_3AH_6 and AH_3 (gel or crystalline), the relative proportions depending on the hydration conditions and curing period. At lower temperatures CAH_{10} and C_2AH_8 (both hexagonal phases) and AH_3 gel are preferentially formed, and at higher temperatures are converted to C_3AH_6 and gibbsite. Most attempts to explain strength gain or loss have related to the relative amounts of calcium aluminate hydrate in the hydrated products. Formation of C_3AH_6 has been associated with strength decrease, although under certain conditions increased strength has been obtained (1)

Applications of HAC include sulphate-resistant cements, bore hole plugging cements, fast-setting patching compounds, rock anchors, grouting, cold temperature concreting, and refractories. Recently, HAC has been used instead of $CaCl_2$ as an accelerator.

In the past decade fibre-reinforced cement composites having a variety of cement-based matrices and organic and inorganic fibres have proved particularly useful in some repair applications. Within 24 h HAC develops high compressive strength and appears to be a good candidate for such applications. Fibre-reinforced cement composites, when compared to unreinforced systems, generally have increased flexural strength and fracture toughness, i.e., resistance to crack initiation and propagation. As the matrix plays an important role in composite behaviour, knowledge of its fracture properties is necessary for understanding that behaviour. There is, however, a dearth of information on fracture of non-portland cements and for HAC systems there appear to be few published data.

The possibility of using microhardness measurements to predict fracture mechanics parameters in non-porous solids, e.g., soda-lime glass, has been explored with some success (2,3). The objective of the present study was to obtain experimental data on the fracture behaviour of HAC and to investigate the possible dependence of several fracture mechanics expressions (critical values of stress intensity factor, strain energy release rate, J-integral, work of fracture) on microhardness.

Indentation Fracture

This section is included to provide a basis for the expectation of a dependence of fracture properties on microhardness. The principles and applications of indentation fracture have been reviewed, principally by Lawn and Wilshaw (4) and only a few salient points will be discussed. The cardinal features of Lawn and Wilshaw's approach, upon which fracture mechanics analysis was based, are:

(1) the sharp point of the indentor produces an inelastic deformation zone;

(2) a deformation-induced flaw suddenly develops into a small crack (called median vent) on a plane of symmetry containing the contact axis;

(3) increased load causes further stable growth of the median vent;

(4) on unloading the median vent does not completely close and lateral vents begin to develop.

Figure 1 illustrates vent crack formation under a sharp indentor (4). Calculations approximating the stress field beneath the indentor by a Boussinesq elastic field (excluding the small disturbed zone beneath the indentor) where the depth of the median vent, c, is much greater than the depth of the disturbed zone result in the following expression for strain energy release rate:

$$G = (1-\nu^2) \left[(1-2\nu)^2/2\Pi^4 \right] (\alpha/\beta^2) (H/E) \ P/c \qquad (1)$$

where G is strain energy release rate, ν is Poisson's ratio, E is modulus

MICROHARDNESS, FRACTURE, ALUMINATE CEMENT

FIG. 1

Schematic of Lawn's model of vent crack
formation under point indentation. Dark
region is inelastic deformation zone (2)
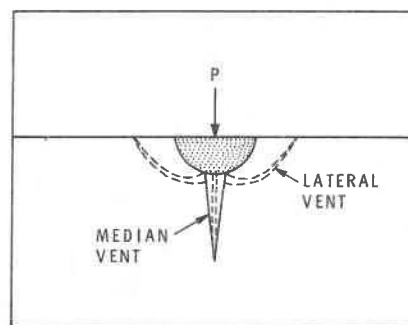
of elasticity, H is microhardness, P is applied load and α and β are
dimensionless geometrical factors.

The ratio P/c has been found to be constant. For many porous cementitious
materials E and H are empirically related by an expression of the form
$E = kH^n$ (k and n are constants) (5). Thus, it might be expected from
eq. (1) that G would be related to microhardness through a power law
relation. It is assumed that the crack is ideally Hookean and that linear
elasticity theory applies, and, therefore, linear elastic fracture mechanics
(LEFM).

Application of Fracture Mechanics to Cement Paste Systems

The majority of fracture mechanics studies of cement paste systems,
usually portland cement paste, have been conducted in the last decade (6).
Data are often conflicting, and there is disagreement concerning the applica-
bility of LEFM and the relative merits of expressions describing fracture
behaviour. There is also disagreement concerning the crack propagating
mechanism in cementitious materials. The basic issue is one of brittleness
versus ductility in the crack tip zone. There are two major schools of
thought. One assumes an ideally sharp crack in which fracture proceeds by
progressive rupture of cohesive bonds across a separation plane, creating new
surface area in a reversible manner. The other school postulates that the
macroscopic "plastic-zone" concept describing the crack tip region of some
metals and polymers is applicable to ceramic materials on a microscale. The
controversy remains unresolved. There appears to be, however, a universal
concensus that, whatever the extent of the validity of LEFM to brittle frac-
ture, the information gathered has been valuable in both characterizing
materials and providing input to the design process.

Some critics have suggested that fracture terms calculated using maximum
load values (obtained from load-deflection curves) are essentially indicators
of resistance to crack "initiation" and do not necessarily assess resistance
to crack "propagation." The total work of fracture, however, determined by
integration of both ascending and descending branches of load-deflection
trace, reflects resistance to both crack initiation and propagation.
Integration of areas under the ascending branch only reflects resistance to
crack initiation.

Experimental

Materials

The composition of the HAC was as follows: $Al_2O_3 = 40.02\%$;
$Fe_2O_3 = 17.71\%$; $CaO = 37.26\%$; $SiO_2 = 3.46\%$; $MgO = 0.91\%$; $SO_3 = 0.08\%$;
$Na_2O = 0.08\%$; $K_2O = 0.08\%$. Blaine fineness was 394 m^2/kg.

J.J. Beaudoin

Eight series of samples were prepared. Each consisted of a set of samples for the following water/cement ratios: 0.25, 0.30, 0.35, 0.40, 0.45 and 0.50. Mixes were cast in moulds 1.2 × 7.5 × 20 cm that were fitted with metal shims 0.6 × 0.025 cm thick (running the length of the mould) to provide a precast crack in the specimen. The samples were removed after 3 days at 100% RH and sawn at 0.127 cm intervals along their length to produce the final test specimens. Thus, the test piece was a beam 1.2 cm deep × 0.127 cm thick × 7.5 cm long with a mid-span notch 0.025 cm wide × 0.6 cm deep. All beam samples were stored at 11% RH for a minimum of 14 days prior to testing or pretreatment.* Various treatments are summarized in Table I. Their objective was to produce systems having varied amounts of hexagonal and cubic phases.

The systems were characterized using a differential scanning calorimeter (DSC). Within each series the ratio of peak heights at approximately 300 and 140 to 155°C was kept constant.** Endothermic peaks at 300 and 140 to 155°C represent the thermal decomposition of cubic and hexagonal phases, respectively. In series 1 to 5 the peak at 140 to 155°C decreased with length of heat treatment at 80°C due to dehydration of CAH_{10}.

Technique

DSC

Differential thermograms of the samples were obtained by DSC supplied as a module to Du Pont 900 thermal analysis system. This unit utilizes chromel-constantan thermocouples for differential temperature measurement. The reference material was ignited $\alpha-Al_2O_3$ and the heating rate 20°C min^{-1}. The differential temperature was registered at a sensitivity of 0.02 mV in.$^{-1}$. Thermograms were obtained in air, and in each experiment 20 mg of the sample was subjected to analysis.

Microhardness

Hardness was measured with a Leitz miniload tester in a conditioned box (11% RH) free of CO_2 using the Vickers pyramid indentor. Five determinations were performed on the surface of each sample.

Fracture Testing

An environmental chamber (Fig. 2) was mounted on the cross-head of an Instron testing machine (10,000 kg capacity). Notched beam specimens conditioned to 11% RH were simply supported in it and loaded at the mid-point. The mid-span deflection was measured using an LVDT with a readout accurate to 0.0001 mm. The cross-head speed was 0.005 mm/min. Load-deflection curves were obtained from the Instron chart records; the maximum loads were generally less than 1 kg (the stiffness of the Instron machine is extremely large relative to the flexural stiffness of the test pieces).

---

*Strength and fracture of hydrated cements are humidity dependent. The 11% RH condition minimizes the risk of carbonation, further hydration, excess volume change and is a convenient reference state.

**This was achieved by pre-selecting treatment times from the results of time sequential DSC runs, i.e., treatment times for samples were increased incrementally until the desired DSC peak ratio was attained.

MICROHARDNESS, FRACTURE, ALUMINATE CEMENT

TABLE I

Description of Sample Treatments for Fracture Studies

Series	Treatment	Composition**
1	100% RH, 3 d; 11% RH, 21°C	Very little cubic phase
2	100% RH, 3 d; 11% RH, 21°C; vacuum 3 h, 80°C; 11% RH	Mostly hexagonal in order 1 2 3 4 5
3	100% RH, 3 d; 11% RH, 21°C; vacuum 6 h, 80°C; 11% RH	
4	100% RH, 3 d; 11% RH, 21°C; vacuum 24 h, 80°C; 11% RH	
5	100% RH, 3 d; 11% RH, 21°C; vacuum 21 d, 80°C; 11% RH	
6*	100% RH, 3 d; 11% RH, 21°C; 100% RH, 80°C; 11% RH	Cubic and hexagonal approximately equal
7*	100% RH, 3 d; 11% RH, 21°C; 100% RH, 80°C; 11% RH	Approx. 80% cubic 20% hexagonal
8	100% RH, 3 d; 11% RH, 21°C; autoclaved, 216°C; 11% RH	Mostly cubic

*For series 6 and 7 the times at 100% RH, 80°C, varied with water/cement ratio from about 10 to 25 min.   Series 7 was treated for longer periods.

**Approximations made by estimating DSC peak heights at 300°C

Following is a description of the expressions defining the conditions of fracture and their method of determination from load-deflection curves:

(1) K_c: Stress intensity factor, K, has been described as a single-parameter description of the stress and displacement fields in the region of the crack tip. The critical stress intensity factor, K_c, is the value of K for unstable fracture.

For mid-point loading of single edge-notched flexural specimens (7)

$$K_c = Y \, 3/2 \left(P_{max} \ell \sqrt{a} \right) / \left(b \cdot d^2 \right)$$

where

$$Y = 1.93 - 3.07 \, a/d + 14.53 \, (a/d)^2 - 25.11 \, (a/d)^3 + 25.8 \, (a/d)^4$$

P_{max} = maximum load; ℓ = length of beam; a = length of notch;
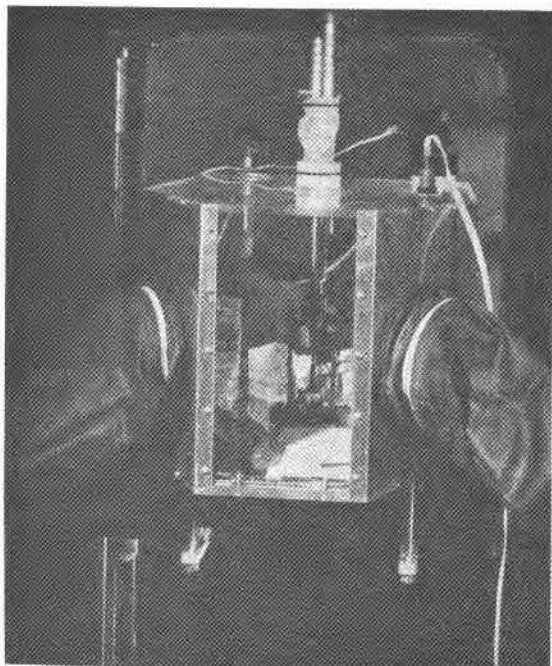
b = beam width; d = beam depth.

J.J. Beaudoin

FIG. 2

Fracture-testing arrangement
showing environmental chamber
mounted on cross-head of
Instron machine

(2) G_c: Strain energy release rate, G, is a material constant depending on
the physical processes occurring at the crack tip and is equal to twice
the fracture surface energy per unit area. Critical strain energy
release rate is designated G_c.

The dependence of compliance (ratio of centre-span deflection to load)
on crack length was determined at each water/cement ratio for every
series. For a given crack length samples were loaded to about 70% of the
maximum during each loading cycle. After a compliance determination the
crack was extended using a saw and the compliance for the new crack was
determined. G_c was calculated according to the following expression:

$$G_c = P_{max}^2 \left(dC/da \right)/2b$$

where

P_{max} = maximum load; C = compliance; a = crack length;

b = beam width.

(3) J_c: J is a path independent line integral describing the crack tip
stress-strain field intensity under elastic-plastic conditions. For
elastic bodies the critical value of J-integral equals G_c, i.e.,
$J_c = G_c$.

This calculation requires load-deflection curves for both notched and
unnotched samples.

$$J_c = (2/b.d) \left\{ An - Au \right\}$$

where

An = area under load-deflection curve up to maximum load, P_{max}
for notched sample;

Au = area under load-deflection curve of the unnotched sample up
to the maximum load, P_{max}, which was determined for the
notched sample;

b = specimen width.

(4) Work of fracture, γ_T: This term is determined by dividing the area
under the total load-deflection curve by the area of the uncracked beam
ligament $(b.\{d-a\})$. γ_T represents the work of fracture for crack
initiation and propagation. The area under the ascending portion of the
load-deflection curve can also be determined, and when this area is
divided by the uncracked ligament area an estimate of the work of
fracture for crack initiation, γ_i, is obtained.

FIG. 3

Plot of stress intensity factor,
K_c versus microhardness for
various HAC preparations
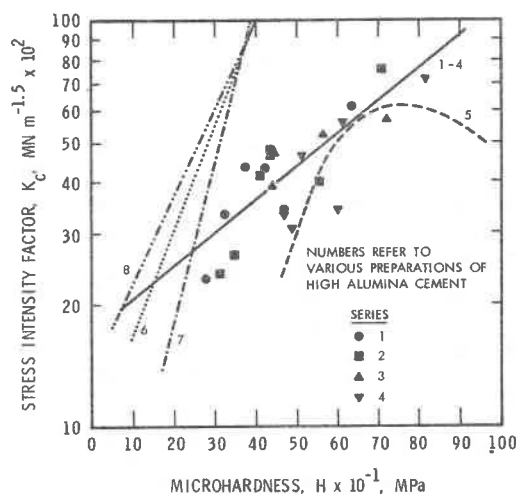
Observations

Dependence of Fracture Terms on Microhardness

Fracture terms, K_c, G_c, J_c and γ_T, are plotted against
microhardness, H, for series 1-8 preparations (Figs. 3-6). There is a linear
dependence of logarithms on microhardness for many of the terms; some depen-
dences are non-linear. Regression analysis for the linear curves is presen-
ted in Table II, and can generally be described as follows: semi-log plots
of K_c, G_c and J_c versus H for series 1 to 4 are linear, and values of
these terms increase with microhardness. One curve for each fracture term
fits the data for series 1 to 4. A semi-log plot of γ_T versus H for series
1 is also linear. All other log γ versus H curves (series 2 to 8) are non-
linear and increase to a maximum value, then decrease as H increases. The
log $(K_c, J_c, G_c, \gamma_T)$ versus H curves for series 5 are non-linear and
generally increase to a maximum value as H increases; for γ_T and G_c they
subsequently decrease with increasing H. The curve, log K_c versus H for
series 8, is linear and log K_c increases with H. Log (J_c, G_c, γ_T)
for system 8 increases, however, to a maximum and then decreases as hardness
increases. Log (K_c, G_c, J_c) versus H curves for series 6 and 7 are
also linear and each curve has a greater slope than the curve for series
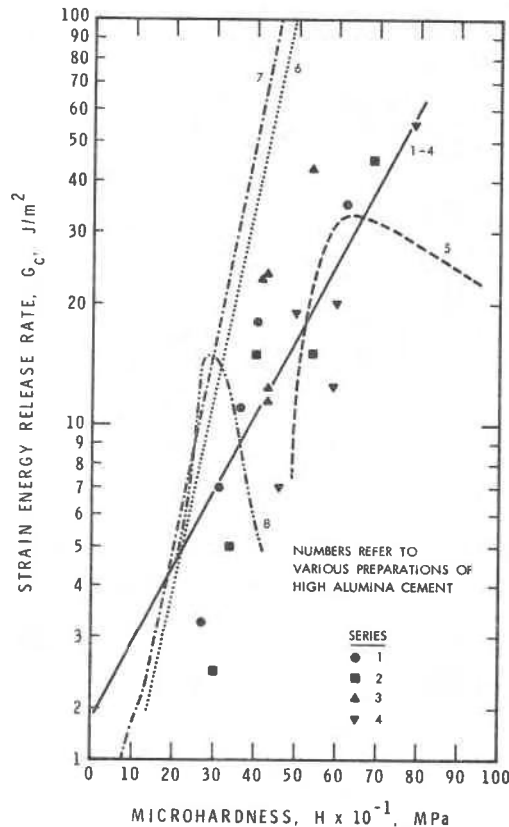1 to 4.

J.J. Beaudoin

FIG. 4

Plot of strain energy release rate versus microhardness for various HAC preparations

Discussion

In this study fracture terms (K_c, G_c, J_c) for HAC systems are dependent on microhardness, in agreement with measurement of indentation fracture of non-porous ceramic bodies. Hydrated HAC systems containing mixtures of hexagonal phases and cubic phases had larger increases in these fracture terms for an equivalent microhardness change than the systems consisting mainly of hexagonal phases alone.

A possible explanation of this behaviour is that the denser cubic phase (density of C_3AH_6 = 2.52; CAH_{10} = 1.75) occurs as finely dispersed inclusions that modify the stress field in the material and act as crack arrestors. The (K_c, G_c, J_c) versus microhardness curves for the mixed morphology preparations cross the curves for preparations consisting mainly of hexagonal phases. At lower microhardness values mixed morphology systems have lower fracture values, possibly owing to the relative ease of crack initiation and propagation through weak areas at points of interparticle contact.

The rate of change of K_c with hardness for the preparation containing mainly cubic phase is also greater than the mainly hexagonal systems. G_c and J_c for the cubic material increase with hardness in the same manner as do the mixed morphology systems, but decrease at higher microhardness values. The decrease may be due to pore-crack interaction. Fracture toughness may be dependent on crack-arresting properties of pores as well as on total porosity (8). Values of K_c for some porous ceramics, e.g., beryllium, increase to a maximum and then decrease as strength increases (9).

TABLE II

Regression Analysis of Fracture-Microhardness Data

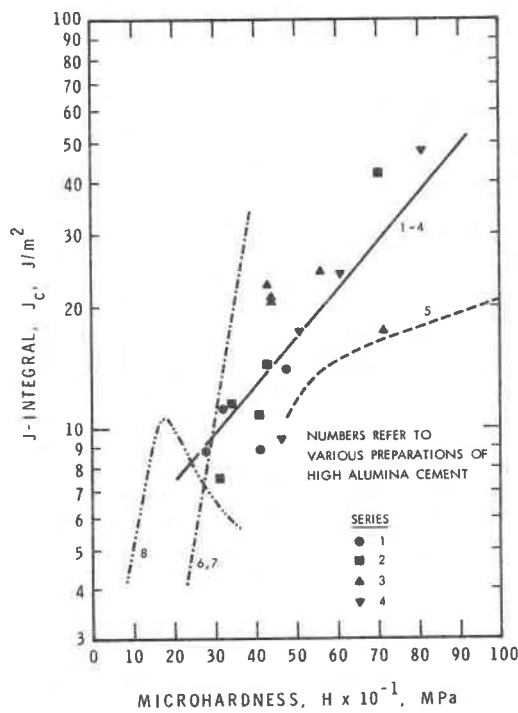| Series	Regression Equation	Correlation Coefficient (r)
1-4	$K_c = 16.86 \exp (0.019) H$	80.1
	$G_c = 1.88 \exp (0.041) H$	72.5
	$J_c = 4.29 \exp (0.027) H$	75.5
1	$\gamma_T = 6.12 \exp (0.026) H$	71.4
6	$K_c = 9.33 \exp (0.060) H$	91.5
7	$K_c = 2.08 \exp (0.101) H$	85.5
8	$K_c = 14.45 \exp (0.046) H$	96.0
6	$G_c = 0.51 \exp (0.104) H$	71.0
7	$G_c = 0.71 \exp (0.099) H$	72.0
6,7	$J_c = 0.19 \exp (0.124) H$	96.0

FIG. 5

Plot of J-integral versus
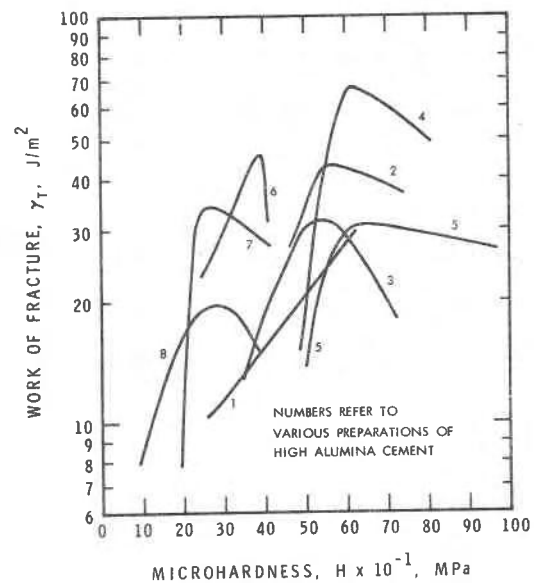microhardness for various
HAC preparations

FIG. 6

Plot of work of fracture versus
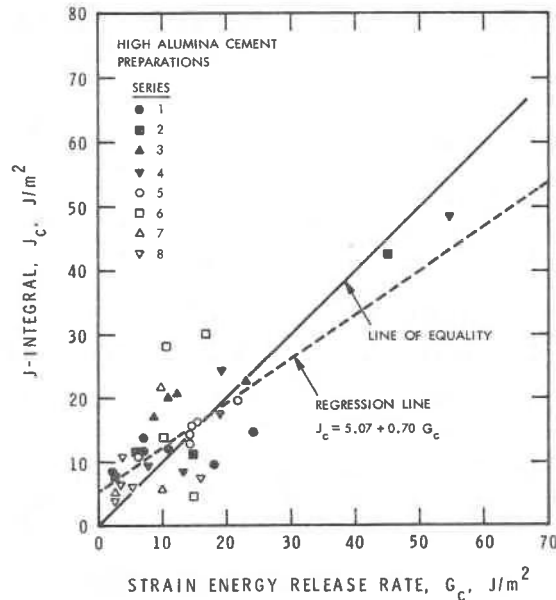microhardness for various HAC
preparations

J.J. Beaudoin

FIG. 7

Plot of J-integral versus strain
energy release rate for various
HAC preparations

It is apparent that in cement systems microstructural features, e.g.,
porosity, pore structure, density, crystallinity and morphology, may affect
the dependence of the fracture terms on microhardness. Two pieces of
evidence support the application of linear fracture mechanics and the bond
rupture process for the materials studied.

(1) Measured values of G_c for ceramic materials and for the HAC systems
studied approach values of 2γ within a factor of two or three (see
Table III). G_c is several orders of magnitude in excess of 2γ for
metallic and polymeric materials, which fracture according to a plastic
crack-tip separation process.

(2) Ideally, if linear elastic processes are involved in fracture,
$J_c = G_c$. Figure 7 is a plot of J_c versus G_c for the HAC
systems. The data points are positioned about the "line of equality."
Regression analysis gives a line, $J_c = 5.07 + 0.700\ G_c$ with
correlation coefficient = 79.3%.

TABLE III

Ratio of G_c/γ for Various Materials

Reference Materials					HAC Series*							
Si	Ge	SiC	$A\ell_2O_3$	SiO_2	1	2	3	4	5	6	7	8
1.76	1.83	4.00	4.00	7.77	0.84	0.88	0.81	1.22	0.87	0.87	1.50	0.80

*Values for each series are average values for various w/c preparations

Conclusions

1. There is a relation between fracture behaviour of high alumina cement
    systems and microhardness. This means that it may be possible to
    estimate the values of the fracture terms from microhardness
    measurements.

2. The relation between the fracture terms and microhardness is dependent on
    the morphology of the hydration products.

3. Mixed morphology (hexagonal and cubic phases) systems have greater
    fracture toughness than systems containing mainly hexagonal phases except
    at low values of microhardness.

4. Non-linear relations between logarithms of work of fracture and micro-
    hardness are obtained for most systems. Non-linearity may result from
    energy dissipation processes due to pore-crack interaction.

5. Approximate equivalence of J-integral and strain energy release rate
    supports the assumption that linear elastic fracture mechanics is applic-
    able high alumina cement paste systems.

References

1. V.S. Ramachandran and R.F. Feldman. Cem. Concr. Res. $\underline{3}$, 729 (1973).

2. B. Lawn and E.R. Fuller. J. Mats. Sci., $\underline{10}$, 2016 (1975).

3. B. Lawn and M. Swain. J. Mats. Sci., $\underline{10}$, 113 (1975).

4. B. Lawn and R. Wilshaw. J. Mats. Sci., $\underline{10}$, 1049 (1975).

5. J.J. Beaudoin and R.F. Feldman. Cem. Concr. Res. $\underline{5}$, 103 (1975).

6. S. Mindess. Mats. Res. Ser. (2), University of British Columbia, p. 95
    (1981).

7. B. Gross and J. Srawley. ASTM STP 410, 13 (1966).

8. R.W. Rich. In Treatise on Materials Science and Technology, Vol. 11,
    Acad. Press, Chapt. 4, 1977, p. 200, (ed. by R.K. MacCrone).

9. R.E. Cooper. Atomic Weapons Research Establishment, Report 017/72, U.K.,
    Atom. Ener. Auth. 40, (1972)

Acknowledgement